Overview of T-10 Results.

D.A. Kislov for the T-10 Team

NFI RRC "Kurchatov Institute", Moscow, Russia

E-mail: dkislov@nfi.kiae.ru

Abstract. Essential progress has been made in understanding the links between energy and particle transport and plasma turbulence behavior in T-10 plasma with electron cyclotron heating (ECH). High-density plasmas with the energy confinement time that attains the H-mode scaling predictions have been obtained with gas puffing and ECH. Interplay between evolution of the plasma confinement with density and turbulence properties related to ion temperature gradient and trapped electron modes has been studied. Degradation of the energy confinement with an increase of ECH power coincides with the growth of the turbulence level in the low magnetic field side, while it has been found to be almost unchanged in the high magnetic field side. Successive deuterium pellet injection can result in improvement of the energy confinement over the H-mode scaling predictions. Formation of electron internal transport barrier has been observed during the current ramp-up phase with ECH. Experimental study of sawtooth control by electron cyclotron current drive near q=1 surface has been performed and the optimal profile of the driven current has been found.

1. Introduction

The primary objective of T-10 experimental program is to explore and understand the physics of confinement and stability in plasmas with powerful electron cyclotron heating (ECH) and current drive (ECCD). Confinement studies with ECH address physics that governs plasma transport under the conditions when the main heating power is transfered to the electron component that is character of the reactor plasma with α-heating. Feasibility to control the location and the radial width of power deposition region makes ECH/ECCD a powerful tool for safety factor (q) profile control, allowing us to address issues in physics of ITB formation and MHD stability.

T-10 is a tokamak with circular cross-section (major radius R_0=1.5m, minor radius a=0.3m) which is operated with toroidal field $B_t \leq 3T$ and plasma current $I_p \leq 0.45MA$. The characteristic feature of T-10 tokamak is the dominant electron heating provided by the ECH system. At present, ECH system consists of five gyrotrons with total heating power up to 2.5MW: 1.2MW at 130GHz and 1.3MW at 140GHz (second electron cyclotron harmonic, low field side injection, extraordinary wave mode). ECH system provides highly localized power deposition (minimum width of power absorption profile is $\approx$2% of the minor radius, power density up to 25W/cm^3 is achievable). The cut-off density is $n_{cut-off}$=1.2*10^{20}m^{-3} for power injection that is perpendicular to the tokamak magnetic axis. The value of the driven current in T-10 experiments in the case of EC power injection at an angle to the major radius was found to be close to the linear theory predictions with the maximum ECCD efficiency $\eta_{CD}=I_p n_{e20} R/P_{ECH}$=0.013AW^{-1}m^{-2} for EC second harmonic.

This paper concentrates on the main recent results on interplay between energy and particle confinement and plasma turbulence behavior in T-10 plasma (Section 2), on improvement of the energy confinement due to successive deuterium pellet injection and effects concerned with pellet penetration in plasma (Section 3), on internal transport barrier formation during the current ramp-up with ECH (Section 4) and on studies of sawtooth control by ECCD (Section 5).

2. Confinement and turbulence studies

Essential progress has been made in understanding the links between energy and particle transport and plasma turbulence properties. The energy confinement time τ_E increases with plasma density $\bar{n}_e$ almost linearly up to $\bar{n}_e \leq 0.6 n_{Gw}$ in T-10 L-mode regimes with gas puffing. The τ_E growth saturates at higher densities ((Fig. 1(a)). Nevertheless, the τ_E values exceed L-mode scaling (ITER L-96 [1]) predictions ((Fig. 1(c)) and attains the H-mode scaling (IPB98(y,2) [1]) predictions ((Fig. 1(d)) at $\bar{n}_e > 0.6 n_{Gw}$. We note, that L- and H-mode scaling predictions are similar for the conditions of the experiment in T-10 (τ_{EH}/τ_{EL} $\approx 2.44 * B_t^{0.12}(T) * R^{0.14}(m) * A^{-0.64}$, A=R/a=5). Transport analysis of experimental data shows that the confinement saturation at high densities results from a decrease of energy stored in electron component (Fig. 1(b)) that cannot be explained only by a combined effect of an increase of the energy transferred from electrons to ions and an increase of the radiated power [2].

An increase of the density peaking factor with plasma density $\bar{n}_e$ has been observed both in OH and ECH regimes (Fig.2a). This corresponds to an increased density peaking with growing collisionality factor ($\nu_{eff} = \nu_{ei}/\omega_{De}$, where ω_{De} is the curvature drift frequency) (Fig.2b). We note that the ratio of electron temperature to ion temperature (T_e/T_i) ratio changes from 10 at low densities ($\bar{n}_e \approx 0.2 n_{Gw}$) to 2 at high densities ($\bar{n}_e \approx n_{Gw}$) for the operating conditions of the experiment. The phenomenon of density pumpout (flattening of the density profile with an increase of power transmitted to electron component) has been observed in all

FIG. 1. (a) Energy confinement time τ_E; (b), total (W_{tot}) electron (W_e), and ion (W_i) stored energies (c),(d) enhancement factors $H_L = \tau_E/\tau_{L-96}$ and $H_H = \tau_E/\tau_{IPB98(y,2)}$ versus plasma density (I_p=200kA, B_t=2.5T, P_{ECH}=0.9MW).
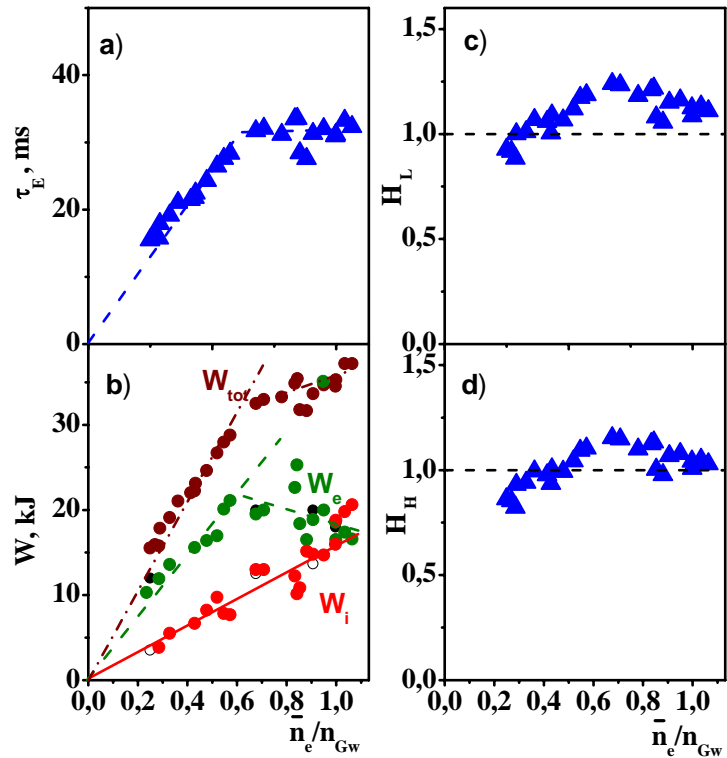
range of collisionalities investigated (see also Ref. [3]) (It is worth noticing reduction of density peaking factor in the L-mode with respect to OH shown in Fig. 2).

Analysis of the drift turbulence stability has been made to estimate possible turbulence contribution to the energy and particle transport in T-10. According to calculations by linear electrostatic code KINEZERO [4] both trapped electron mode (TEM) and ion temperature gradient (ITG) mode exist in the low density region ($\bar{n}_e \leq 0.6 n_{Gw}$) in the L-mode plasma. According to calculations by RITM code [5] for the high density region, analytical estimation of the turbulence growth rates and contribution of the different turbulence types to plasma transport [6] TEM mode dominates in the whole range of densities, while ITG mode was found to be stable or close to the stability margin for $\bar{n}_e > 0.6 n_{Gw}$. The ETG mode is predicted to be unstable in the region of the energy confinement saturation and possibly contributes to the increase of electron energy losses at high densities. Density peaking at low collisionalities observed in ASDEX-U [7] has been explained with the anomalous inward pinch considered in the framework of the ITG/TEM model for the case of ITG domination. Domination of TEM looks to be the possible reason for the lack of the density peaking at low collisionalities in T-10 experiments. We note, that the loop voltage increases with collisionality in these experiments (from 0.4V to 1.2V) and the increased contribution of the Ware pinch into an inward particle transport can be expected. Domination of TEM looks to be consistent also with the observation of the density pumpout in the whole range of collisionalities. Thus, an increase of power transferred to electron component due to ECH can result in TEM drive that is able to give rise to an outward particle flux [8].

Particle transport was studied using KCl and Ti pellet injection and perturbative technique of fast deuterium gas puffing [9]. The impurity transport was analyzed by means of X-ray crystal monochromator [10]. Characteristic times of deuterium and impurity dynamics have been found to be comparable with the τ_E values and have the same density and ECH power tendencies in OH and L-mode plasma. Degradation of characteristic time of titanium impurity dynamics and the energy confinement time with increasing ECH power is illustrated in Fig.3. These experimental observations may suggest the dominant role of turbulence convection

FIG. 2. Density peaking factor (ratio of line integrated densities nl(0.15a)/nl(0.8a)) for OH and L-mode plasma vs (a) plasma density (b) effective collisionality (I_p=200kA, B_t=2.5T, P_{ECH}=0.9MW).
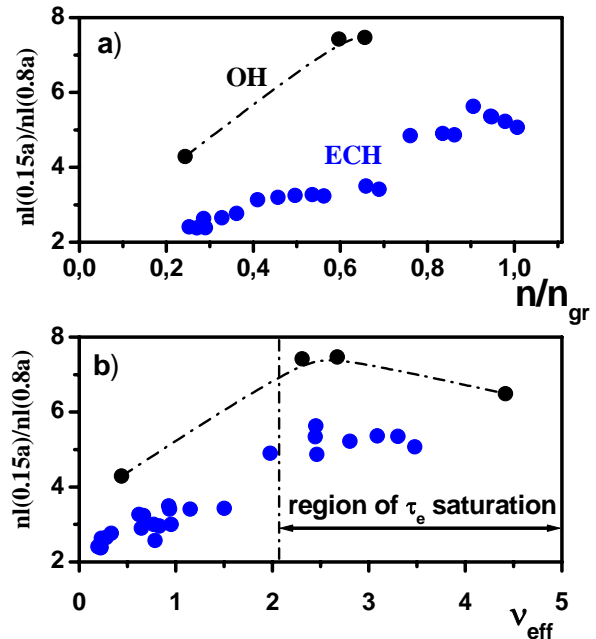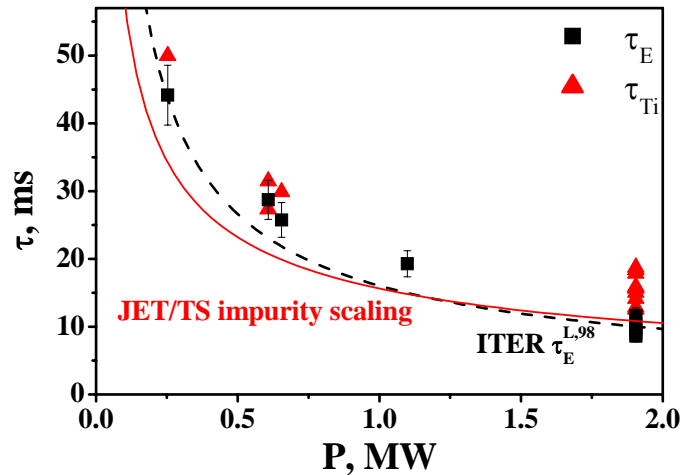
FIG. 3. Dependences of energy (black squares) and Ti^{20+} (red triangles) confinement times from total power in discharge with $I_p = 200$ kA. ITER L-mode (black) [1] and JET/TORE SUPRA [11] scalings are shown.

both in ion and electron channels. It should be noted that τ_E values have been obtained in steady state, while characteristic particle times were derived roughly from dynamical experiments.

According to classification of the turbulence fluctuation types measured using correlation reflectometry and Langmuir probes five components in the turbulence spectrum are possible to distinguish in T-10 plasma [12]. The core spectrum includes background Broad Band (BB) fluctuations, High Frequency (HF) and Low Frequency (LF) Quasi Coherent (QC) spectral maxima (typically at frequencies 70-120kHz and 150-200kHz respectively) and Low Frequency (LF) peak in the region of zero frequency (Fig. 4). SOL fluctuations have a single spectral maximum at zero frequency. Besides that, analysis of Langmuir probe data shows that high density structures with radial size 0.5-3cm and poloidal size 2-3cm are formed and propagates in radial and poloidal directions in SOL [13]. The observed high density structures can be responsible for more than 50% of the total radial turbulent flux in SOL.

Experimental data are found to be consistent with the hypothesis, that the origin of LF and HF QC is ITG and TEM instabilities respectively. Good agreement was found between radial locations of LF and HF QC fluctuations and radial locations predicted for of ITG and TEM instabilities correspondingly [12]. The $k_\perp \times \rho_i$ values approach 0.3 for LF QC and 0.7 for HF QC, that is close to theoretical predictions for ITG and TEM. According to the data from T-10, TEXTOR and FTU the value of $k_\perp \times \rho_i$ for LF QC in core regions was found to be independent on toroidal field in the range from 1.5 to 8T [14] that is consistent with theoretical predictions for the ITG mode. A possible reason for QC fluctuations is helical fingers formation due to toroidal mode coupling [15]. The BB activity can be attributed to the stochastic excitation of single modes. Thus, QC fluctuations possibly indicate a type of the instability that dominates in BB. It is also worth noting that LF fluctuations could be related to "streamers" due to its long radial correlation lengths with zero phase shift.

Tendency of the transformation of a turbulence spectrum with characteristic LF QC peak to a spectrum with characteristic HF QC peak with density increase has been observed both for OH and L-mode plasma. The peak related to low LF QC fluctuations is seen on the frequency spectra at low densities (Fig. 4). The LF QC related peak decreases at higher densities and the peak related to HF QC arises. LF QC fluctuations completely vanish at densities where confinement growth saturates. Relative QC maxima decrease at high ECH power that is seen in the bottom panels of Fig. 4. In spite of a decrease of QC maxima with ECH these
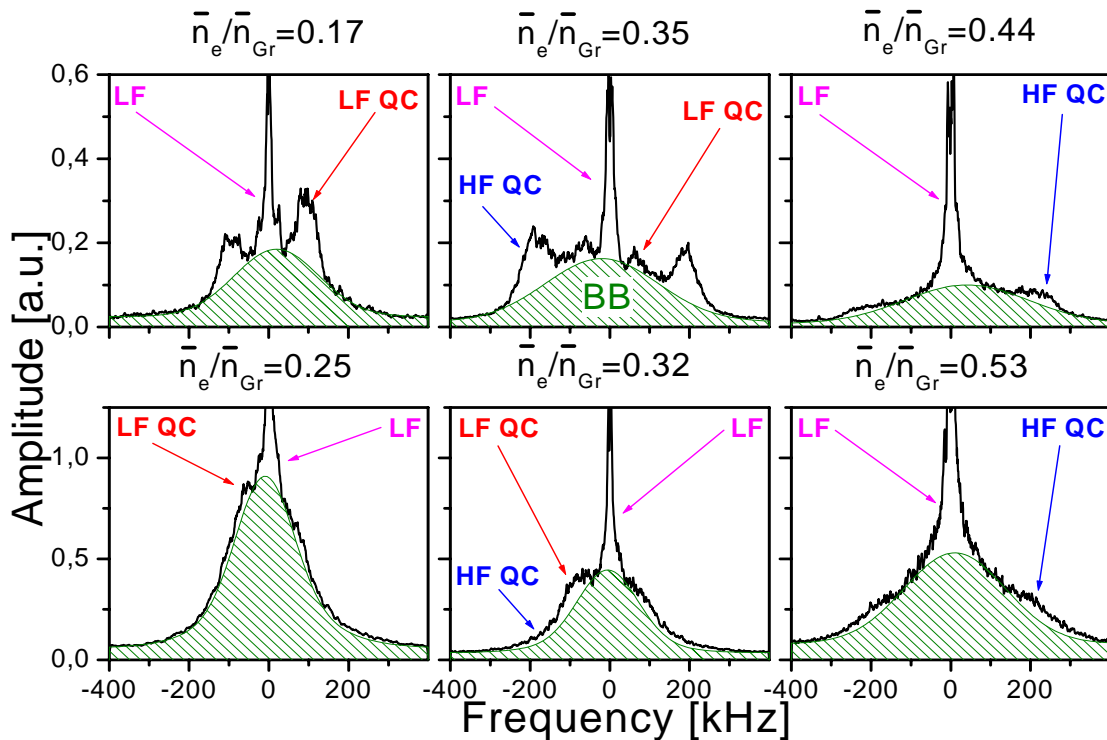
FIG. 4 Fourier spectra amplitudes of reflected signal at $\rho \approx 0.5$ in OH discharges (top) and in discharges with ECH (bottom). The BB parts of spectra are shown as shaded regions.

fluctuations are clearly distinguishable due to coherency measurements. The total turbulence level increases significantly due to ECH power injection that is the typical feature of the confinement degradation in the L-mode. This could occur due to the transition of the turbulence from the linear or quasi-linear regime, to the strong non-linear stage, where all the linear features are concealed.

Thus, general good agreement between the hypothesis that LF and HF QC peaks indicate existence of ITG and TEM in plasma correspondingly and tendencies of the turbulence stability in the calculations has been found. The response of the LF QC fluctuations to the density peaking looks to be consistent with ITG stabilization with an increase of the density gradient. ITG mode was found to be stable in RITM calculations, while LF QC completely vanishes in the high density region. Existence of TEM in the region where the τ_E growth saturates correlates with the observations of characteristic HF QC peak. However, domination of TEM in the energy transport in the low density region observed in the calculations looks as a contradiction with the lack of HF QC peak at low densities.

Evolution of plasma turbulence across the major radius with ECH power injection has been investigated [9] with the recently installed HFS extraordinary wave mode reflectometry system [16] and LFS ordinary mode reflectometry system [12]. Strong asymmetry in the amplitude of the density fluctuations has been found in OH. (The amplitude of the density fluctuations in the LFS has been found to be higher than the amplitude in the HFS by a factor of 2-3.) However, typical spectrum components have been observed in the HFS. Surprisingly, the changes of the turbulence amplitude in the HFS have been found to be negligible with ECH power injection, while it increases strongly in the LFS (Fig. 5). The amplitude of the

turbulence in the LFS increases mostly due to BB oscillations, while the contrast of the QC peaks decreases with ECH power injection.

FIG. 5. Radial profile of relative electron density perturbations amplitude in OH and ECH discharges with $I_p = 300 \, \kappa A$, $B_T = 2.45T$, $\bar{n}_e = 3 \times 10^{19} cm^{-3}$, $P_{ECH} = 1.5 \, MW$.
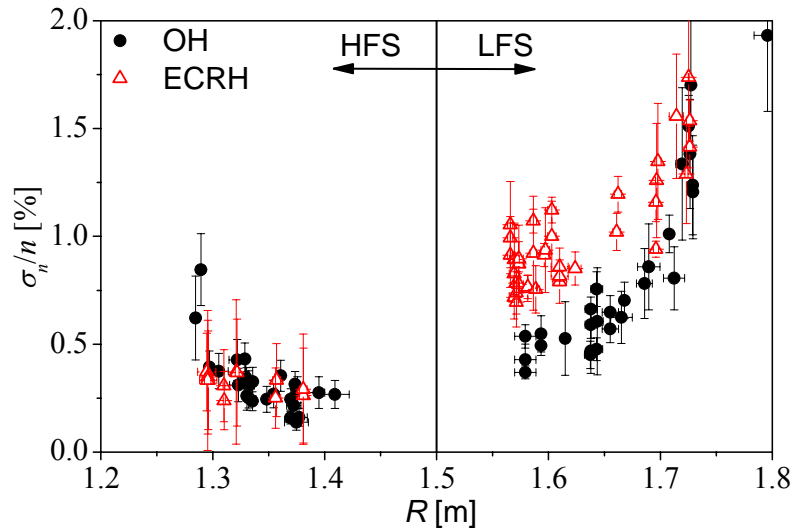
3. Pellet injection effects

Successive deuterium pellet injection in low edge safety factor regimes ($q_a \approx 2.5$) results in an improvement of energy confinement with respect to its "saturated" level of gas puffing regimes (Fig. 6) [17]. The regimes with the pellet injection are characterized by essentially increased density peaking factor with respect to the gas puffing regimes, increased neutron yield and $T_i(0)$. Confinement enhancement $H_H = \tau_E/\tau_{IPB98(y,2)}$ factor attains $H_H = 1.3$ with successive injection of five pellets (the maximum number of pellets available). The pellets were injected from the LFS. The regimes with the highest τ_E values obtained with injection of 4-5 pellets have the characteristic features of pellet enhanced confinement (PEC) mode reported earlier [18]. (The PEC mode was observed with injection of a single pellet in plasma with relatively low density ($\bar{n}_e \approx 0.3 n_{Gw}$) in a few shots with improved wall conditioning.) The observed improvement of confinement with deuterium pellet injection was found to be reduced with an increase of the edge safety factor.
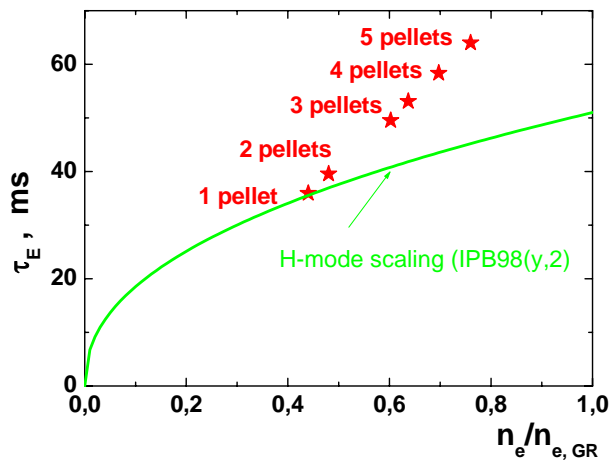

FIG. 6. Energy confinement time τ_E attained in the shots with different number of deuterium pellets versus plasma density ($I_p=300kA$, $B_t=2.4T$, $P_{ECH}=1.4MW$).
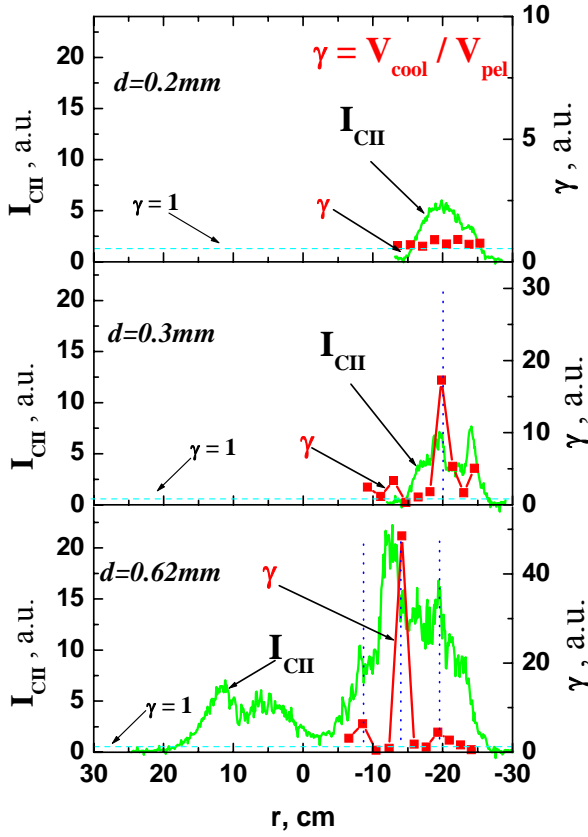
FIG. 7. The ratio of the cooling front velocity to the pellet velocity (γ) and I_{cII} pellet radiation power (that is proportional to the ablation rate) for carbon pellets with sizes d=0.2mm, 0.3mm and 0.62mm. (I_p=270kA, B_t=2.4T, $\bar{n}_e$ =2*$10^{13}cm^{-3}$).

Processes of fast particle and energy transport initiated by deuterium or impurity pellet are under study [19]. Local regions where the velocity of cooling fronts formed by pellets (measured by ECE diagnostic) considerably exceeds the pellet velocity have been observed (Fig. 7). These regions correlate well with bursts/drops of the pellet ablation rate. Threshold effect of pellet size has been observed for these phenomena. Sawtooth reconnection event triggered by a pellet crossing the q=1 surface region that assists and accelerates particle penetration into plasma center has been observed both with deuterium and impurity pellet injection. This sawtooth reconnection event corresponds to the region of the cooling wave acceleration in the central part of the plasma column. Hypothesis, that regions of the cooling wave acceleration and decreased pellet ablation are concerned with MHD reconnections in the outer part of plasma has been proposed in Ref. [19].

4. Electron internal transport barrier formation with ECH during current ramp-up

Formation of electron internal transport barrier (ITB) has been observed during the current ramp-up phase with ECH applied for "freezing" the safety factor profile (q(r)) [20]. Application of ECH during the current ramp-up phase can result in considerable transient increase of electron temperature in the central part of plasma (r/a<0.35) in the current flat-top over its value in the conventional T-10 L-mode with similar parameters. Traces of central electron temperature ($T_e(0)$) (from second harmonic electron cyclotron emission diagnostic (ECE)) for T-10 L-mode shot (ECH at the current flat-top) and for a shot with the same plasma parameters and ECH applied in the current ramp-up phase are shown on Fig. 8. Differences of the density profiles for these two shots are inside experimental accuracy. Electron ITB is formed in the region 0.1<r/a<0.35 in the shot with early ECH. This region with increased (with respect to the L-mode value) T_e gradient, $\rho_{Te}=\rho_s/L_{Te}$ value (ρ_s is the local
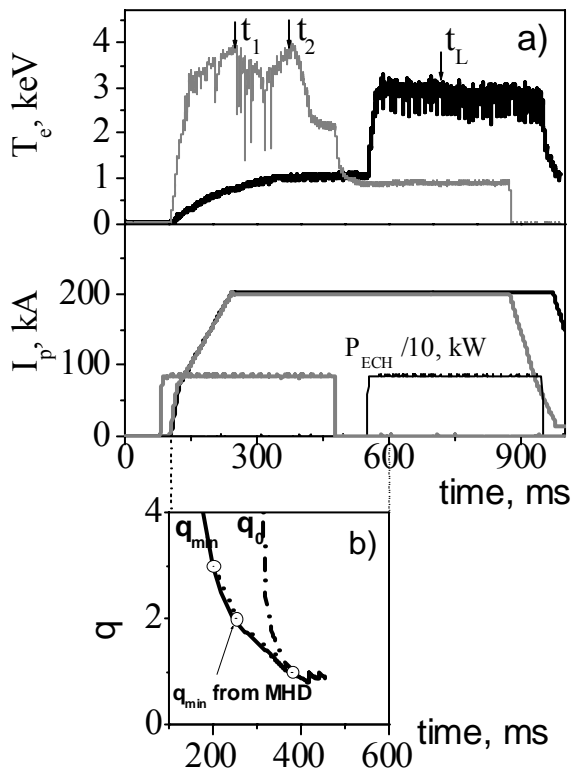
FIG. 8. Central electron temperature ($T_e(0)$), plasma current (Ip), ECH heating power (P_{ECH}) in shots with ECH in the current ramp-up – gray lines and ECH in the current flat-top – black lines. ($\bar{n}_e=2*10^{13}cm^{-3}$, $B_t=2.5T$, $P_{ECH}=1MW$) b) q_0 and q_{min} from calculations in the shot with ECH in the current ramp-up.

ion Larmor radius at the speed of sound, L_{Te} is the electron temperature gradient scale length), that can be used to characterize the ITB quality [21], and decreased effective electron thermal conductivity (χ_{eff}) obtained by interpretative calculations [20] by ASTRA transport code [22] exists in plasma until m=1/n=1 activity starts (Fig. 9).

Evolution of q(r) profile in the shot with ECH during the current ramp-up phase has been simulated using ASTRA code. According to the simulation the ITB is formed in the conditions of nonmonotonic q(r) with $q_{min}>3$. As it is seen on Fig. 8 an MHD onset that
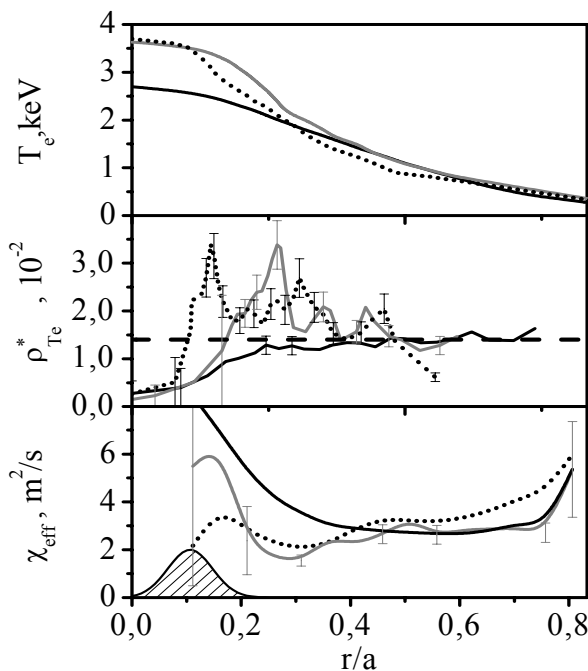

Fig. 9 Profiles $T_e(r)$ profiles, $\rho_{Te}(r)$, $\chi_{eff}(r)$, profiles for t_1(dot line), t_2 (gray solid) and t_L (black solid line) on Fig.8. Location of ECH power deposition is shown by filled area.

correlates with ITB deterioration occurs when q_{min} crosses a low order rational value. ITB disappears when q_{min} value falls below unity and magnetic shear becomes positive across the minor radius.

Analysis of drift turbulence stability in plasmas with the ITB formation has been performed [23] using linear electrostatic code KINEZERO [4]. The long wavelength turbulence (TEM, ITG) was found to be stable inside r/a<0.35 (position of the ITB foot) in the early stage of discharge when q_{min} >2, and its increment was found to be strongly reduced with respect to the L-mode level during the last stage of the ITB existence. According to the calculations short wavelength turbulence (ETG) is stable in the whole range of the parameters investigated. Analysis of the turbulence stability allows us to suppose that stabilizing influence of the reversed shear is the key ingredient in the process of the ITB formation in the experiment with ECH during current ramp-up. It is worth noting that ITBs events (abrupt nonlocal reduction of transport) observed after off-axis ECH switch-off are also under investigation [24]. These ITB events are possibly involved by transient formation of low magnetic shear regions during evolution of safety factor profile after off-axis ECH switch-off. The role of low-order rational surfaces in ITB formation is discussed in Ref. [3].

5. Sawtooth control by ECCD

Electron cyclotron heating and current drive can be considered as a possible technique for sawtooth control in ITER [25]. Experimental study of sawtooth control by ECH and ECCD has been performed for better understanding the physical nature of its influence on sawtooth stability and for optimization of the power usage. In contrast to experiments with sawtooth suppression by ECCD due to a global redistribution of the current profile in the central part of the plasma column reported earlier [26] the recent experiments have been performed with ECH power deposition in a narrow zone ($w_{ECH} \approx (0.03-0.06)a$) near q=1 surface. The plasma column was swept across the major radius during the ECH pulse (P_{ECH}=0.4MW) in order to obtain the dependence of the sawtooth period on the location of the power deposition profile with respect to q=1 surface. (ECH power was deposited in the HFS of the torus.) Dependencies obtained with this technique have been found to be in a good agreement with dependencies obtained in shot to shot variation of B_t.

Considerable stabilizing effect (sawtooth period increases by a factor of up to 9 with respect to OH value) has been observed when the current driven in the direction of the plasma current due to ECH power injection (co-ECCD) is localized in a narrow region near q=1 surface (Fig. 10a). It is worth noting that the profile of the driven current ($j_{cd}(r)$) calculated by Fokker-Plank code OGRAY [27] was found to be considerably wider than the region where ECCD strongly affects sawtooth activity. The width of $j_{cd}(r)$ profile under the conditions of the experiment is comparable with an accuracy of its location with respect to q=1 surface. Thus, in contrast to ASDEX-U experiments [28] we cannot determine whether the optimum location of $j_{cd}(r)$ is at q=1 surface or slightly outside it. ECCD in the direction opposite to plasma current direction (counter-ECCD) localized in the vicinity of q=1 surface produces destabilizing effect (Fig. 10b). The optimum location for destabilizing influence of counter-ECCD was found to be the same as in the case of stabilizing effect of co-ECCD.

Optimized profile of $j_{cd}(r)$ for sawtooth control under the conditions of the experiment has been found. The strongest co-ECCD effect on sawtooth stability has been observed with toroidal angle of power injection in the range 4-8° (Fig. 11). According to calculations by Fokker-Plank code OGRAY this range corresponds to the maximum density of the driven
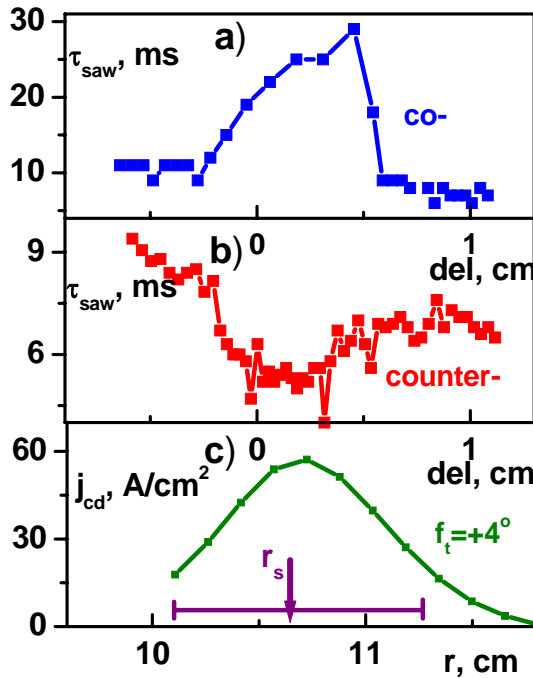
Fig. 10. Sawtooth period (τ_{saw}) vs relative shift of plasma column across the major radius for a) co-ECCD b) counter-ECCD c) jcd(r) profile calculated by OGRAY code (I=230kA, $\bar{n}_e$=1.5*10^{13}cm^{-3}, B_t=2.3T, P_{ECH}=0.4MW)

current in the experiment. Further increase of toroidal angle results in an increase of the total driven current, but the density of the driven current decreases and maximum sawtooth period falls. It is worth noting that considerable stabilizing effect has been observed with small toroidal angles of power injection (1-2)°.

Experiments with opposite directions of the plasma current have been performed in order to define the toroidal angle accurately for comparison between effects of EC heating and current drive on sawtooth activity. ECCD effect in the range 1-16° of toroidal angles of power injection was found to be much stronger than the effect of EC heating alone (in the case of zero toroidal angle).
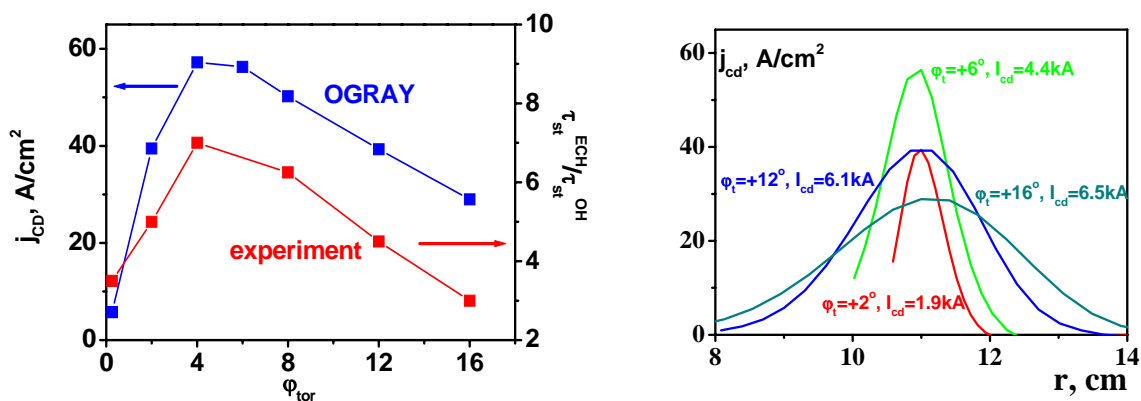

Fig. 11 a) Maximum $j_{cd}(r)$ value from OGRAY calculations and maximum sawtooth period τ_{saw} vs toroidal angle b) $j_{cd}(r)$ profiles from OGRAY calculations with different toroidal angles of ECH power injection.

Localized ECCD can affect the dynamics of the magnetic shear in the vicinity of q=1 surface during a sawtooth that could be expected to have a strong influence on sawtooth stability. Thus, this effect has been observed in calculations [29] that use the critical shear criterion introduced in Ref. [30]. According to simulations with ASTRA code sawtooth behavior in the case of co-ECCD in T-10 experiments has been found to be in a good qualitative agreement with the model that uses the critical shear criterion. However, possible two dimensional effects concerned with the driven current inside magnetic island cannot be excluded.

Conclusion

Essential progress has been made in understanding the physics that governs energy confinement in plasma with dominant electron heating. Detailed study of plasma turbulence allows us to establish links between turbulence properties and transport phenomena observed in T-10 plasma. Operating mode of improved confinement obtained by successive deuterium pellet injection and electron internal transport barrier formation with ECH during current ramp-up have been observed in T-10. ECCD have been proved to be a powerful tool for sawtooth control.

References

[1] ITER Physics Basis 1999 Nucl. Fusion **39** (1999) 2137.
[2] ESIPCHUK Yu. V. et al Plasma Phys. Control. Fusion **45** (2003) 793.
[3] RAZUMOVA K.A. et al Plasma Phys. Control. Fusion **48** (2006) 1373.
[4] BOURDELLE C. et al, Nucl. Fus. **42** (2002) 892.
[5] TOKAR M.Z. et al Phys. Rev. Lett. **84** (2000) 895.
[6] KIRNEVA N.A. et al Proc. 30th EPS Conf. on Cont. Fusion and Plasma Phys., St-Petersburg, 2003, ECA Vol27A, P-3.113, http://epsppd.epfl.ch/StPetersburg/PDF/P3_113.PDF
[7] GÜNTER S et al Nucl. Fusion **45** (2005) S98.
[8] ANGIONI C. et al Nucl. Fusion **44** (2004) 827.
[9] VERSHKOV V.A. et al, this conference, EX/P4-38.
[10] VERSHKOV V.A. et al "Pribory and Technika Experimenta", **6**, 1987, 171 (in Russian).
[11] MATTIOLI M., et al, Nuclear Fusion, **35** (1995) 1115.
[12] VERSHKOV V.A. et al, Nuclear Fusion, **45** (2005) S203.
[13] KIRNEV G.S. et al., Nucl. Fusion **45** (2005) 459.
[14] VERSHKOV V.A. et al "Studies of tokamak core small-scale turbulence in different regimes of T-10, TEXTOR and FTU tokamaks" Proc. 31st EPS Conference on Plasma Phys., London, UK (2004), ECA Vol.28G, O-2.06(2004).

[15] LIN Y. Plasma Phys. Comtrol. Fusion **43** (2001) L1-L8.

[16] D.A. SHELUKHIN et al, 2006, Proc. 33th EPS Plasma Phys. Conf., P.4-081.

[17] PAVLOV Yu. D. et al, this conference, EX/P3-11.

[18] PAVLOV Yu. D. et al in Fusion Energy 2000 (Proc. 18th Int. Conf. Sorrento, 2000), IAEA,   Vienna (2001), CD-ROM file EXP5/17 and http://www.iaea.org/programmes/ripc/physics/fec2000/html/node1.htm

[19] KUTEEV B.V. et al JETP Letters **84** (2006) 295.

[20] KIRNEVA N.A. et al Plasma Phys. Control. Fusion 47 (2005) 1787.

[21] TRESSET G. et al Nucl.Fusion **42** (2002) 520.

[22] PEREVERSEV G.V. et al ASTRA – an Automatic System for Transport Analyses in a Tokamak, Rep. IAE-5358/6, Kurchatov Inst., Moscow (1992).

[23] KIRNEVA N.A. et al, 2006, Proc. 33th EPS Plasma Phys. Conf., P.4-086.

[24] NEUDATCHIN S.V. et al, this conference, EX/P1-8.

[25] MUKHOVATOV V. et al Plasma Phys. Control. Fusion **45** (2003) A235.

[26] KISLOV D.A. et al in Controlled Fusion and Plasma Physics (Proc. 22nd Eur. Conf. Bournemouth, 1995), Vol. 19c, Part I, European Physical Society, Geneva (1995) 369.

[27] ZVONKOV A.V. et al Plasma Phys. Rep. **24** (1998) 389.

[28] MÜCK A et al Plasma Phys. Control. Fusion **47** (2005) 1633.

[29] ANGIONI C. et al Nucl. Fusion **43** (2003) 455.

[30] PORCELLI F, BOUCHER D, ROSENBLUTH M.N. Plasma Phys. Control. Fusion **38** (1996) 2163.